Clays and Clay Minerals, Vol. 33, No. 6, 473–482, 1985.

STRUCTURE AND GROWTH MECHANISM OF GLAUCONITE AS SEEN BY HIGH-RESOLUTION TRANSMISSION ELECTRON MICROSCOPY

MARC AMOURIC

Centre de Recherche sur les Mécanismes de la Croissance Cristalline
CNRS—Campus de Luminy, Case 913, 13288 Marseille cedex 09, France

CLAUDE PARRON

Laboratoire de Géologie Dynamique et Laboratoire associé au CNRS
no. 132, Faculté des Sciences Saint-Jérôme, 13397 Marseille cedex 13, France

Abstract—The internal fabric of glauconite pellets has been studied by high-resolution transmission electron microscopy (HRTEM) for a better understanding of the glauconitization process. Typical "lamellae" which make up the glauconite pellets showed a spindle-like arrangement of layered crystallite packets. Three main mineral phases were detected: (1) well-ordered glauconite *sensu stricto* (d(001) = 10 Å) generally in the middle of the spindles; (2) a poorly ordered and undetermined layered-phase "X" with d(001) ~12.5 Å, usually sandwiching glauconite such that the interface between the two materials is very sharp; and (3) a noncrystalline or gel-like phase located between the lamellae. A 14-Å smectite-like phase was rarely observed at the periphery of some grains. The glauconite crystallites clearly showed characteristic growth features (e.g., growth steps), whereas the unknown phase X exhibited destabilization characteristics. A structural analysis of the pure glauconite indicates that this dioctahedral mica was present in the 1*Md* (disordered), 1*M*, and, to a much lesser extent, $2M_1$ polytypic forms. HRTEM revealed no interlayering of glauconite with the other layered phases. Rather, it appeared to have formed by a layer-growth mechanism at the expense of the unknown phase X which apparently converted into noncrystalline matter before converting to glauconite. The precursor function of the interlamellae "gel" phase during the evolutive process of glauconitization is not understood.

Key Words—Glauconite, Growth mechanism, High-resolution transmission electron microscopy, Mica, Polytype.

Résumé—La structure interne de grains de glauconie provenant de roches sédimentaires paléocènes de Côte d'Ivoire, a été étudiée par la microscopie électronique en transmission à haute résolution (METHR) afin de mieux comprendre le processus de glauconitogenèse. Les lamelles typiques, observées au microscope électronique à balayage, qui composent la glauconite, révèlent en METHR une organisation en fuseaux ou navettes constitués de paquets de cristallites à structure en feuillets. Trois phases principales ont pu être détectées: (1) La glauconite s.s. bien ordonnée (d(001) = 10 Å) au coeur des fuseaux; (2) une phase mal ordonnée et indéterminée (phase X), telle que (d(001) ~ 12,5 Å), entoure communément les paquets de cristallites de glauconite; et (3) une phase non cristallisée, ressemblant à un gel, localisée entre les lamelles. Une phase à 14 Å de type smectitique a pu être rarement observée à la périphérie de certains grains.

L'analyse structurale des cristallites de glauconite indique que ce mica dioctaédrique présente le plus souvent les formes polytypiques 1*M* et 1*Md* et moins fréquemment la forme $2M_1$ mise en évidence ici pour la première fois. Concernant les relations entre les différentes phases observées, la METHR ne révèle aucune interstratification des feuillets de glauconite avec les autres phases. Les cristallites de glauconite montrent clairement des figures caractéristiques de croissance (gradins par exemple) aux endroits ou la phase X présente des caractères de déstabilisation, tels que sa transformation en un matériau pauvrement cristallisé ou amorphe. Ainsi l'étude en METHR des grains de glauconie révèle que la glauconitisation constitue un processus évolutif au cours duquel le premier stade cristallisé semble représenter par la formation, peut être à partir d'un gel, d'une phase X en feuillets à 12,5 Å (smectite Fe ou nontronite?). La cristallisation de la phase glauconitique, par un mécanisme de croissance par couches, suit la déstabilisation (amorphisation) de la phase à 12,5 Å. Ces nouvelles observations militent fortement pour la théorie de la néoformation de la glauconite plutôt que pour la "layer-lattice theory".

INTRODUCTION

Green glauconitic pellets found in marine sedimentary rocks show considerable mineralogical variability. According to X-ray powder diffraction and chemical data, the dominant mineral in glauconite grains is generally thought to be an iron-rich, mixed-layer mineral, structurally similar to interstratified illite/smectite and made up of high-charge, mica-like, non-expandable layers (10 Å) and low-charge, smectite-like, expandable layers (14–15 Å) (Warshaw, 1957; Burst, 1958a, 1958b; Hower, 1961; Bentor and Kastner, 1965).

Based on the Fe content, Velde and Odin (1975)

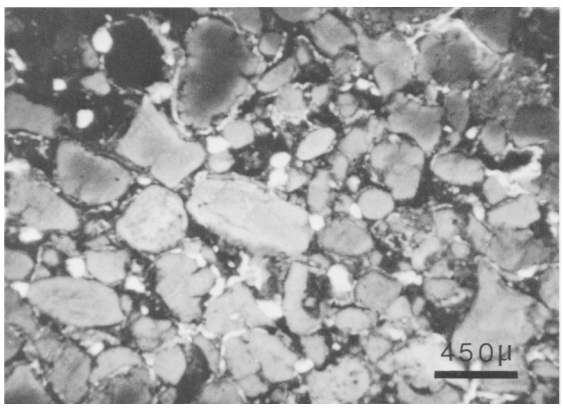

Figure 1. Photomicrograph of the dark-green glauconitic rock made up essentially of various size glauconite pellets, commonly showing internal random aggregate texture and fibro-radiated rims (polarized light).

distinguished illite/smectite mixed-layer material from glauconite/smectite mixed-layer material and suggested that the latter forms a continuous solid solution between smectite and glauconite. The mineralogical diversity of glauconite appears, in any case, to be directly related to the proportion of smectite-like layers, which progressively decreases during the glauconitization process (Hower, 1961; Thompson and Hower, 1975). The end-member of this process is glauconite *sensu stricto,* i.e., a Fe-K-rich, dioctahedral clay-size mica. The mixed-layer model has been rejected by other authors who suggested that the mineralogical and chemical diversity of glauconites results from variations of cation distribution and hydration state in a smectite-like structure evolving towards a mica (Odin, 1975), or in the mica structure itself (Kohler, 1980).

To document interstratification phenomena in glauconite minerals and to produce additional information about the glauconitization process, high-resolution transmission electron microscopy (HRTEM) has been carried out to define the microstructures in glauconite pellets from Paleocene marine rocks of the Ivory Coast.

EXPERIMENTAL PROCEDURES

Samples

The glauconite pellets analyzed belong to Paleocene formations of the Eboïnda region, in the eastern part of the sedimentary basin of the Ivory Coast (Charpy and Nahon, 1978; Nahon *et al.,* 1980; Parron and Nahon, 1980). These formations contain south to north lateral facies changes. Limestones containing phosphatic and glauconitic pellets change within a distance of 30 km into partly bituminous, glauconitic black shales which become progressively more clastic to the north where sands and conglomerates overlie the Precambrian basement. The glauconites examined were collected from these black shales. The shales consist of alternating, millimeter to centimeter thick, layers of black clay and of lenses of dark-green glauconite admixed locally with minute crystals of pyrite.

Examination under the petrographic microscope shows that the rock contains abundant, round, green glauconitic pellets (Figure 1) which make up as much as 90% of the rock and which show a random, microaggregate internal structure and, commonly, fibro-radiated rims. The grains are brown where they are stained by organic matter. The matrix of the glauconite pellets consist of clay minerals oriented parallel to the bedding, and relatively rare angular grains of quartz usually <0.2 mm in size. Clusters of pyrite crystals are locally abundant in the matrix and replace many glauconite pellets, thereby suggesting that the pyrite is later than the various types of glauconite.

Methods

Sample preparation. Fractionation and purification of the green pellets were made as follows: first, the sediment was washed on a 40-μm screen to separate the green pellets from their matrix. The pellets were screened further, and the 125–315-μm size fraction, the richest in pellets, was treated with an electromagnetic separator. A final concentration of the darkest green grains was carried out by hand-picking from the most paramagnetic fraction.

X-ray powder diffraction. X-ray powder diffraction (XRD) data were obtained using CoKα radiation (50 kV, 40 mA) and a Philips PW 1130 diffractometer. The XRD patterns were made on random powder mounts, the quickest and most informative technique relating to the degree of crystallinity of glauconite minerals (Odin, 1975).

Chemical analysis. Chemical analyses for major elements were carried out on two purified fractions of glauconite pellets (125–160 μm and 160–200 μm) having the same high paramagnetic susceptibility and dark-green color. Samples were heated for one night at 100°C and then for 1 hr at 1000°C to determine absorbed and structural water, respectively. Si and Ti were measured by colorimetric methods, the former after alkaline fusion and the latter after dissolution by HF and $HClO_4$. Fe^{2+} was measured by volumetric methods using $K_2Cr_2O_7$. The other elements were determined using a Varian A-A 775 atomic absorption spectrophotometer.

Scanning electron microscopy. A Jeol JSM 35 CF scanning electron microscope (SEM) was used to observe the internal texture of some highly paramagnetic, dark-green glauconite pellets, previously broken.

High-resolution transmission electron microscopy. Because high-resolution transmission electron microscopy (HRTEM) requires a minimum thickness of the specimen (typically <150 Å) parallel to the electron

https://doi.org/10.1346/CCMN.1985.0330601 Published online by Cambridge University Press

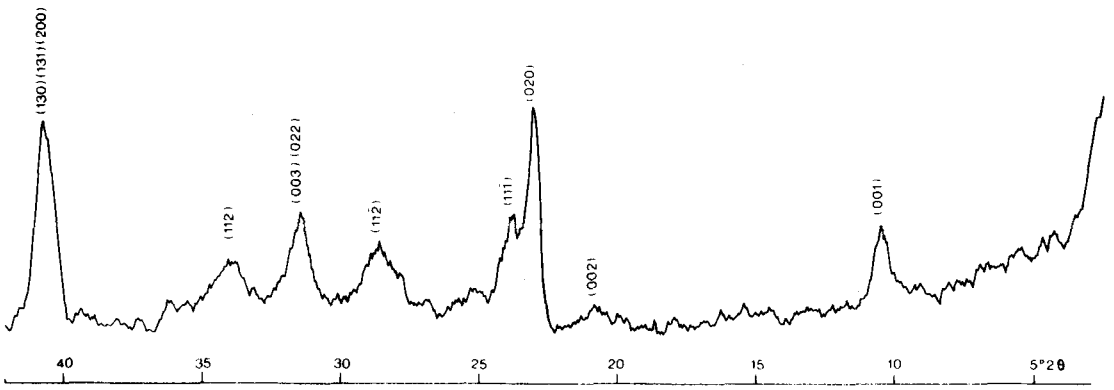

Figure 2. X-ray powder diffraction pattern on random powder of purified dark-green glauconitic pellets (CoKα radiation).

beam, ex-situ and in-situ glauconite grain slices were prepared using ultramicrotoming and ion-thinning techniques. The ultramicrotoming technique was first adapted to clay minerals by Eberhart and Triki (1972) and Tchoubar *et al.* (1973). The glauconite grains selected were embedded in Araldite resin, and the grain-bearing rods were then sectioned using a LKB ultramicrotome equipped with a diamond knife. Only sections below 500 Å in thickness were transferred to carbon-coated copper grids. A drawback of this technique is that the orientation of the grains or of their constituent crystallites cannot be controlled during preparation; however, the highly abundant and randomly oriented crystallites commonly offered adequate diffraction orientation to characterize the principal mineral phases. Observations parallel to the phyllosilicate layers, found to be particularly useful in structural analysis of micas by Amouric *et al.* (1978) and Amouric and Baronnet (1983), were thus made. Even where the ultramicrotoming technique did not preserve the grain-matrix textural relationships, it proved to be the best method to detect noncrystalline phases.

The ion-thinning technique (Phakey *et al.*, 1972; Oertel *et al.*, 1973; Paulus *et al.*, 1975) made use of ordinary petrographic thin sections, 30 μm thick, as starting material. Copper grids, 2–3 mm in diameter, were glued to the rock slice on areas rich in glauconite pellets, previously selected with the petrographic microscope. The glauconite area-grid pairs were then removed from the glass slide and submitted to double-gun argon ion-milling at low beam-incidence angles. At the end of the milling process, the ion accelerating voltage was lowered to minimize ion-beam damage on the specimen. The latter was finally coated with a thin carbon layer (~100 Å thick). TEM observations were made on the thinnest areas of the preparation next to holes. Orientation problems concerning mineral grains were the same as those discussed above for the ultramicrotoming technique because no preferred orientation was present in the rock.

HRTEM imaging conditions. A JEM 100C electron microscope, equipped with a fixed specimen stage and an objective lens pole piece with a spherical coefficient $C_s \sim 1.7$ mm was used in the study. All micrographs were recorded using bright-field illumination. Reflections passing through a 40-μm objective aperture centered on the incident 000 beam at 100 kV contributed to the images. The point-to-point resolution was therefore constrained to ≥ 3 Å. Images were selected from experimental through-focus series recorded in the 800–1200-Å range of underfocusing. The best imaging conditions for glauconite were defined by referring to previous image simulation in micas (Amouric *et al.*, 1981). Inasmuch as quick recording of images was needed to avoid severe electron-beam damage to the specimen, tilting procedures were avoided. As a result, one-dimensional images were mainly analyzed in this work; however, most images showed 00*l* lattice fringes of the principal mineral phases present in the glauconite pellets.

RESULTS

Mineralogical and chemical results

The XRD pattern (Figure 2) reveals a monomineralic composition for the purified glauconite mineral. The basal lattice spacing (d(001) ~ 10 Å), the sharp and symmetrical peaks at 4.53 (020), 3.33 (003), and 2.50 Å (130) and the 111, 112, and 11$\bar{2}$ reflections are evidence indicating an ordered 1*M* mica-like structure (Yoder and Eugster, 1955; Burst, 1958a; Bentor and Kastner, 1965; Odin, 1975) which characterizes glauconite *sensu stricto.* A noticeable broadening of the 111, 112 and 11$\bar{2}$ reflections, however, indicates a significant number of stacking faults within this average 1*M* structure. Moreover, a low-angle broadening of the 10-Å peak suggests the presence of a material having layer spacings >10 Å mixed with glauconite.

The chemical analyses of the two samples of different sized pellets (Table 1) are similar. Both fall within the

https://doi.org/10.1346/CCMN.1985.0330601 Published online by Cambridge University Press

Table 1. Chemical analyses (wt. %) and structural formulae (on basis of 22 oxygen atoms) of glauconite pellets.

Sample	SiO_2	Al_2O_3	Fe_2O_3	FeO	MgO	TiO_2	K_2O	CaO	Na_2O	H_2O+	H_2O-	Total Fe as Fe_2O_3	Total
1 (ϕ125–160 μm)	50.69	7.20	15.43	2.82	4.67	0.20	7.43	0.54	0.58	8.91	1.94	18.56	100.21
2 (ϕ160–200 μm)	49.88	7.05	15.40	3.20	4.78	0.15	7.48	0.56	0.56	9.04	2.11	19.00	100.21

Sample	Tetrahedral		Octahedral				Interlayer				Charge		
	Si	Al	Al	Fe^{3+}	Fe^{2+}	Mg	Ti	Σ	K	Na	Ca	Σ	Tetrahedral	Octahedral	Total
1	3.793	0.207	0.427	0.869	0.176	0.521	0.011	2.004	0.709	0.084	0.043	0.836	−0.207	−0.674	−0.881
2	3.770	0.230	0.398	0.876	0.202	0.538	0.009	2.023	0.721	0.082	0.046	0.849	−0.230	−0.662	−0.881

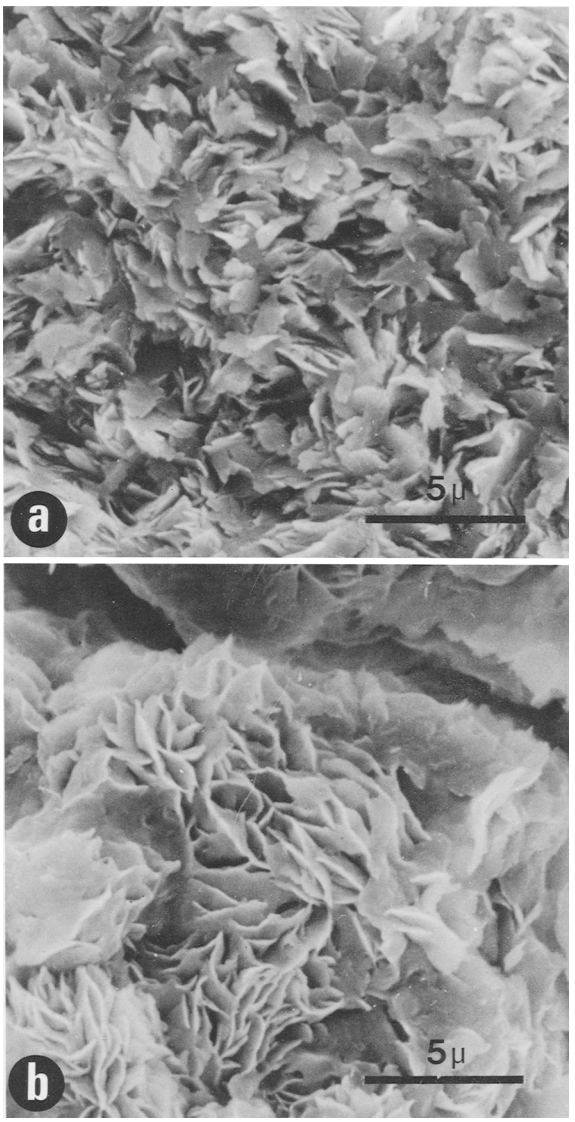

Figure 3. Scanning electron micrographs showing internal aspects of glauconite pellets: (a) typical lamellar arrangement of dark-green pellets; (b) loose stacking aspect of lighter green patches in dark-green pellets.

glauconite compositional range (see compilation by McRae, 1972; Odin, 1975; Kohler, 1980). According to the curves reported by Manghnani and Hower (1964), McRae and Lambert (1968), and Velde and Odin (1975), the K_2O content near 7.5% indicates that the pellets contain fewer than 10% expandable layers. The number of K atoms (0.709–0.721) and the total layer charge (0.88–0.89), on the basis of 22 oxygens (Table 1), confirm the few (5–10%) expandable layers present (cf. Cimbalnikova, 1971a, 1971b; Katsnel'son *et al.*, 1978). Table 1 also provides evidence for an almost perfect dioctahedral nature of the mica.

The dark-green pellets of glauconite displayed a

https://doi.org/10.1346/CCMN.1985.0330601 Published online by Cambridge University Press

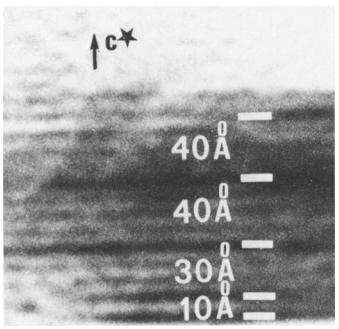

Figure 4. One-dimensional lattice fringe image of a disordered glauconite crystallite. White bars underline the spacing sequence of the aperiodic fringes of this 13-layered mica. Microtomed specimen.

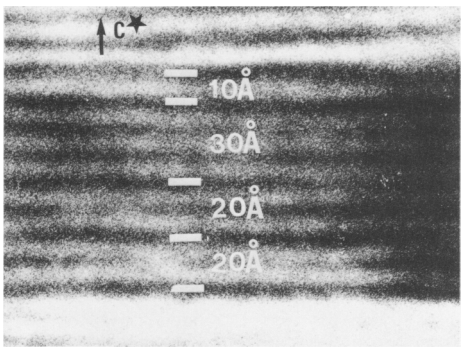

Figure 5. One-dimensional lattice fringe image of a disordered glauconite crystallite. White bars underline the aperiodic fringes spacing sequence of this 8-layered mica. Microtomed specimen.

widespread and characteristic lamellar texture by SEM (Figure 3a). The lamellae, about 3 μm in width and 500 Å in thickness, are arranged in packets which show a fine interlamellar porosity. This kind of lamellar texture was reported by Odin (1974, 1975) as indicative of evolved and highly-evolved grains. Particle size and arrangement differed from one pellet to another as well as within the same pellet. Such changes were reflected as minor variations in the color of the pellets, i.e., lighter green patches corresponded to the loosest stacked lamellae (cf. Figures 3a and 3b).

High-resolution transmission electron microscopy results

Polytypism in glauconite crystallites. Under precise imaging conditions, HRTEM allowed the detailed stacking sequences of the phyllosilicate layers along c* to be seen. Thus, identification of the different polytypic structures that characterize these minerals, crystallite by crystallite, was possible. To check the XRD results, the grains richest in glauconite were sectioned with the ultramicrotome. Several polytypes of glauconite were observed. Figures 4 and 5 are 00*l* lattice fringe images of a 13-layer and an 8-layer mica, respectively. The thickness of the specimen and the departure from an ideal zone-axis alignment prevented a detailed analysis of the stacking sequences being made; however, the fringe contrasts were modulated along c* due to the excitation of "forbidden" diffusion streaks along 00*l* systematics. As shown by Iijima and Buseck (1978), fringes of equal contrast correspond to layers with the same orientation, thereby allowing repeat distances to be measured and stacking faults to be revealed. The darkest fringes are marked by white bars in Figures 4 and 5 where the 10-, 20-, 30-, and 40-Å spacings are clearly visible. No stacking periodicity was noted in these sequences which appeared as disordered (1*Md*) polytypes. This type of aperiodic sequence was commonly observed. Figures 6a and 6b are quasi-structure images of an 11-layer crystallite. Visible white dots, corresponding to the interlayer channels in the structure (Iijima and Buseck, 1978; Amouric *et al.*, 1978), are superimposed with no lateral shift along c* across the crystal. Hence, this well-ordered structure appears to be a pure 1*M* polytype viewed along [100] or [$\bar{1}$00] (Amouric *et al.*, 1978).

Figure 6c shows the corresponding characteristic electron diffraction pattern, in which the 00*l* and 021, 0$\bar{2}$1 reflections contributed to the image. Statistically, this 1*M* structure is as abundant as the 1*Md* structure. Figure 7 illustrates a polytypic sequence rarely observed in this study. The contrast enhancement of the bright fringes every two layers, likely due to the excessive thickness of the specimen, underlines the stacking sequence of this structure along c*. A four-times repeated 20-Å periodicity is visible. This specimen is probably a $2M_1$ polytype of glauconite.

All ordered and disordered, coherent, individual crystallites analyzed by HRTEM in this study constitute, from a polytype point of view, well-structured zones made up exclusively of 10-Å monolayers. These features indicate that the principal phase present is pure glauconite, and that this glauconite may exhibit different, simple-mica polytypic structures.

Relations of different phases in glauconite grains. A wide field micrograph (Figure 8), taken at a mean direct magnification of 100,000, shows the intimate structure of characteristic lamellae of "glauconite" similar to those observed by SEM. In fact, these lamellae appear to consist of a spindle-shaped arrangement of layered crystallite packets. The packets themselves appear to be loosely packed spindles welded to each other by a gel-like noncrystalline material (g) (see also Figure 12a).

Very poorly crystalline matter (A), locally displaying vanishing, unequally spaced linear contrast, coats some spindles (Figure 9), but also exists inside the spindles (Figures 9 and 12a). The spindles themselves are mainly formed by strongly diffracting, well-organized crystallites of glauconite *sensu stricto* (G). They show a 10-

https://doi.org/10.1346/CCMN.1985.0330601 Published online by Cambridge University Press

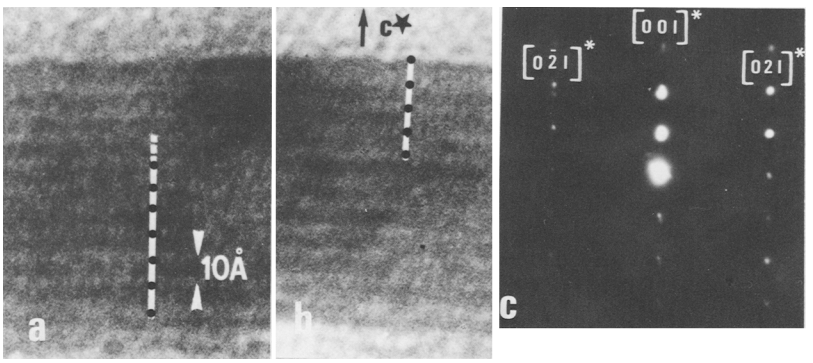

Figure 6. Structure images of an 11-layered glauconite crystallite with a 1*M* sequence viewed along [100] or [$\bar{1}$00]. (a) Left part and (b) right part of this crystallite showing, throughout, its perfect 1*M* polytypic sequence. (c) Corresponding electron diffraction pattern. Microtomed specimen.

Å regular basal spacing and are arranged in sub-grain mosaics with their basal planes parallel or at low angles to each other (Figures 10 and 12a). Each coherent glauconite crystallite consists of a lath commonly 50–150 Å wide and about ten times longer (Figures 10 and 12a).

A poorly organized layered phase (X) (Figures 9, 11, 12a, 12b, 13, and 14) was noted intimately associated with the glauconite. As shown in Figures 9, 11, 12a, and 12b, its poorly organized sheet structure is revealed by blurred, locally interrupted and wavy, lattice fringe contrasts. The mean basal spacing is ~12.5 Å (Figures 11 and 12b). The lattice fringes (X) are parallel to those of adjacent glauconite crystallites (G). Because phase X is poorly crystalline and sensitive to the electron beam, every diffraction pattern recorded after the direct space image shows only glauconite reflections. The 12.5-Å phase sandwiches (Figures 11 and 12b), or, much less commonly, is sandwiched by the glauconite phase (Figures 9 and 13).

The first of these two situations deserves particular attention with regard to the phase X-glauconite interfaces. As clearly shown by Figures 11 and 12b, the interfaces are sharp and smooth. Near the edges of glauconite crystals (G), sharp (growth) steps can be seen (Figure 12b) where the transition with the X-phase structure is present. At each glauconite step the 10-Å lattice fringes appear to be separated from those of the X-phase matrix by a quasi-amorphous region (A), several tens of Ångstrom units in width, into which the 12.5-Å fringes (X) vanish progressively. This transition is also clearly depicted in Figure 14 which shows an elevated step of glauconite, and in the lower part of Figure 13. The second situation is well illustrated in Figure 13 which shows a poorly organized zone (X) vertically squeezed in between glauconite crystallites labeled G1 and G2. The zone appears to consist of a "relic" of the X-phase isolated during the apparent

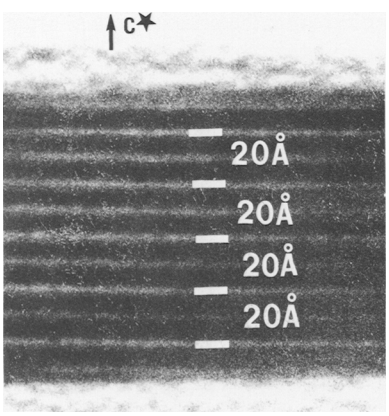

Figure 7. One-dimensional lattice fringe image of a thick section of glauconite. White bars underline the regular $2M_1$ stacking sequence of this small mica. Microtomed specimen.

Figure 8. Transmission electron micrograph showing intimate structure of "glauconite" lamellae. Note spindle-like arrangement of layered crystallite packets and completely noncrystalline zone (g), having a gel-like appearance, between the packets. Ion-thinned specimen.

https://doi.org/10.1346/CCMN.1985.0330601 Published online by Cambridge University Press

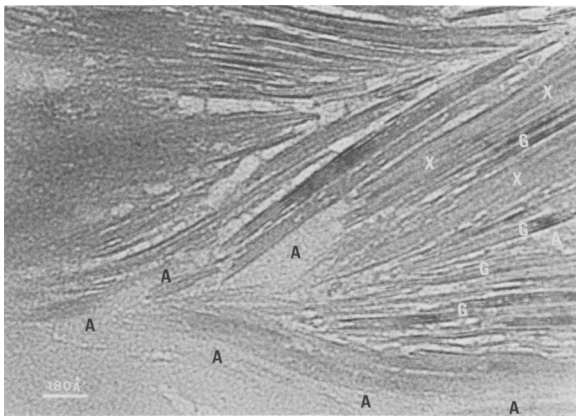

Figure 9. Lattice fringe image of spindle-shaped crystallite packets forming "glauconite" lamellae. Very poorly crystalline matter (A) may coat spindles or be located inside spindles. G = well-organized and contrasted crystallites of glauconite showing 10-Å fringes. X = poorly organized and contrasted layered phase. Ion-thinned specimen.

lateral development of the glauconite. In terms of reacting phases, such microstructures strongly suggest that evolving glauconite is layer-by-layer solid-state growth at the expense of the X-phase matrix.

Noncrystalline areas, similar to the one labelled (g) in Figure 8, can be observed between lamellae. They usually exhibit a mottled appearance and never appear to develop at the expense of the other phases under beam exposure of the specimen. The analysis of such a zone (g) (Figure 12a) reveals no structural organization resembling the phases described above. Neither vanishing Bragg nor lattice fringes nor Moiré pattern were detected inside this noncrystalline phase. Also, no specific corresponding diffraction pattern could be recorded. Nevertheless, the observed contrast (Figure 12a) is significant and suggests the presence of relatively heavy atoms. Such noncrystalline areas resemble a gel; their interlamellar location and wide extension distinguish them from the (A) zones which appeared to be present inside all of the lamellae and which have the characteristics of an X-phase decomposition product.

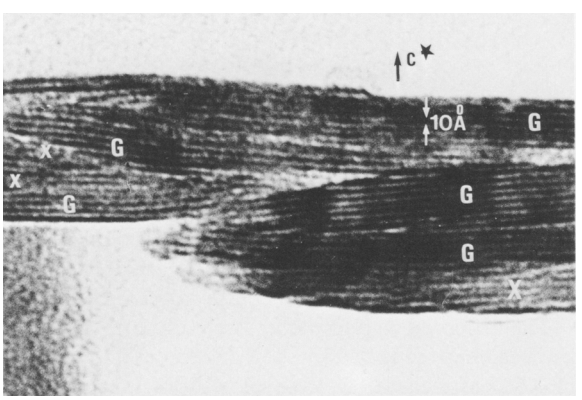

Figure 10. Lattice fringe image of spindles mainly formed by glauconite crystallites *sensu stricto* the basal planes of which are parallel to or at low angles to each other. Crystallites are much more extended in width than in thickness. X = poorly organized phase with ~12.5-Å basal spacing. Microtomed specimen.

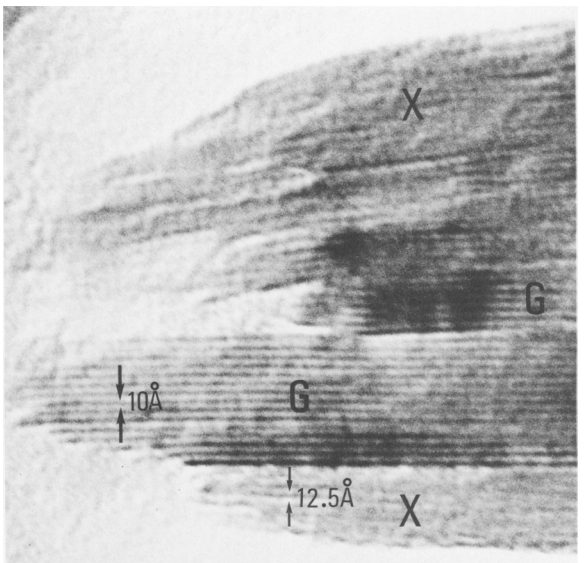

Figure 11. Lattice fringe image of poorly-organized X-phase (d(001) ~ 12.5 Å) commonly sandwiching well-organized glauconite (G) (d(001) ~ 10 Å) in the spindles. 00*l* lattice fringes of X-phase are blurred and discontinuous. Note the sharp and smooth phase X-glauconite interface. Microtomed specimen.

Still another phase has been detected at the periphery of some grains and appears to be a smectite-like structure. Figure 15 shows such a typical sheet-structure stuffed with edge-dislocations, the discontinuous and wavy 00*l* planes of which yield a d(001) of ~14 Å. These features strongly resemble those which characterize the smectic crystals described by De Gennes (1974). The textural relations between this phase and the others is, unfortunately, still unknown.

DISCUSSION

Assuming that only n ($2\pi/3$) (where n = 0, 1, or 2) rotations are possible in the stacking of successive monolayers of mica, the purest glauconite pellets studied show that glauconite appears to adopt three polytypic basic structures, 1*Md*, 1*M*, and $2M_1$. The last polytype was found here for the first time, as a result of HRTEM. All previous studies of this dioctahedral mica reported only the 1*M* and 1*Md* forms. The 1*M* form is the stable form; the second form represents a disordered unstable form (Wise and Eugster, 1964; Ernst, 1963; Burst, 1958a). According to Appelo (1978), the cationic composition of its octahedral sheet (pres-

https://doi.org/10.1346/CCMN.1985.0330601 Published online by Cambridge University Press

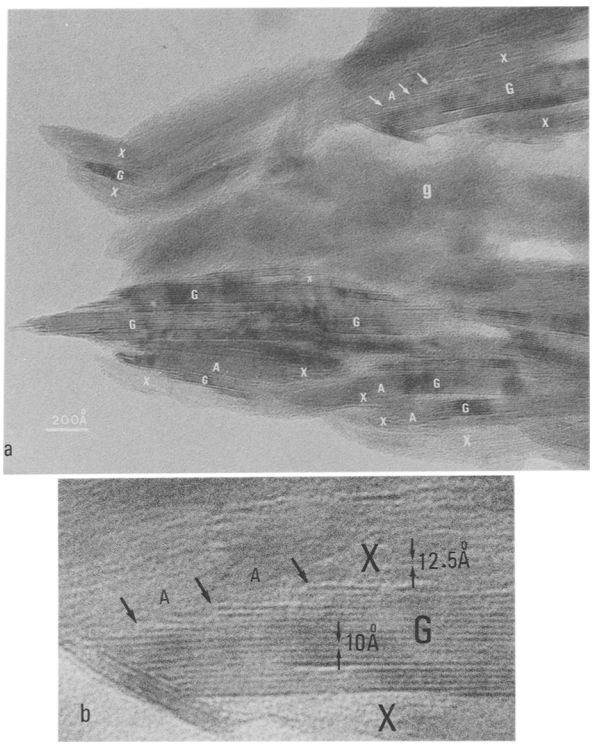

Figure 12. Lattice fringe images of: (a) two close lamellae showing different structural stages separated by a noncrystalline zone strongly resembling a gel (g). G = glauconite, X = phase X, A = very poorly crystalline zones regarded as a decomposition product of the X-phase. (b) Glauconite crystal (G) showing sharp growth steps (arrowed). Adjacent to glauconite steps, note the transition with the X-phase via a very poorly crystalline zone (A). Note also the sharp phase X-glauconite interface and phase X sandwiching the glauconite. Microtomed specimen.

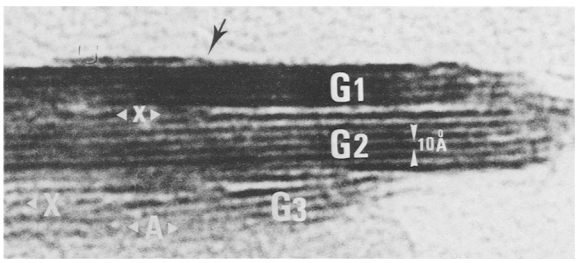

Figure 13. Lattice fringe image of X-phase sandwiched by glauconite. This phase-X "relic" has probably been isolated during the lateral development of glauconite crystals G_1 and G_2. Note the lateral transition glauconite (G_3) to zone A to phase X in lower part of the illustration. Arrow shows a growth step. Microtomed specimen.

ence of larger cations such as Fe^{3+}) causes glauconite to display a polytypic behavior similar to that of trioctahedral micas. Direct lattice imaging suggests that the 1*Md* sequence is related to a pure glauconite structure and not to an interstratified one as was previously assumed (see McRae, 1972).

From a statistical point of view, the frequency of occurrence of these polytypes is $1M \sim 1Md \gg 2M_1$. So-called unstable forms ($1Md$, $2M_1$) are relatively abundant and coexist, even in the same pellet, with the stable form $1M$. The rarity of the $2M_1$ sequence may signify that this form, supposed to be energetically unstable from a structural point of view, is uncommon in separate glauconite crystallites. This scarcity also explains why the $2M_1$ form has never been detected by XRD.

Glauconite crystallites visualized and characterized by means of their basal planes (e.g., d(001) ~ 10 Å) are generally located in a central position inside the spindles. All are well-contrasted, exhibit a regular structural organization, and are clearly individual forms. Growth-steps and important lateral developments are common and are indicative of a fresh phase being generated by a layer-growth mechanism already reported for hydrothermally grown micas (Baronnet, 1974; Baronnet *et al.*, 1976).

This mechanism of glauconite formation, by nucleation and pure growth phenomena, discards the "layer-lattice theory" (Burst, 1958a, 1958b; Hower, 1961), for the phase X to glauconite transformation. The layer-lattice model involves a simple rearrangement in the solid state with incorporation of Fe and K in a smectite-like structure. This structure changes towards a micaceous phase, through smectite/mica mixed-layered intermediates. In the present study, the X-phase (d(001) ~ 12.5 Å), a non-mixed-layered phase, which is significantly different from the 14-Å smectite-like structure found here, forms before the mica appears. Its behavior contrasts with that of the glauconite. The X-phase shows all the characteristics of a progressive destabilization ending with its reduction to a noncrystalline phase. These noncrystalline zones generally mark a front of evolution between the X-phase and the well-structured micaceous phase which grows at the expense of X. Furthermore, the two different phases typically show a parallel or pseudo-parallel orientation of their basal planes. This arrangement can be explained by the fact that the destructuring of the X-phase is easier along the long axis of the layers. Thus, the mica-growth takes place via the noncrystalline zones, in front of the destabilized X-phase. In this way, a global conservation of the spindle and lamellar shapes is possible during the evolution towards a glauconite-mica mineral.

The observed X-phase may correspond to the nontronitic phase reported by several authors on the basis of XRD and chemical analyses to occur during glauconitization (see, for example: Wermund, 1961; Porrenga, 1967; Martin, 1972; Giresse and Odin, 1973; Velde, 1976; Odom, 1976). Complementary chemical microanalyses, now in progress, may answer this question. The revealed layer-growth mechanism observed

https://doi.org/10.1346/CCMN.1985.0330601 Published online by Cambridge University Press

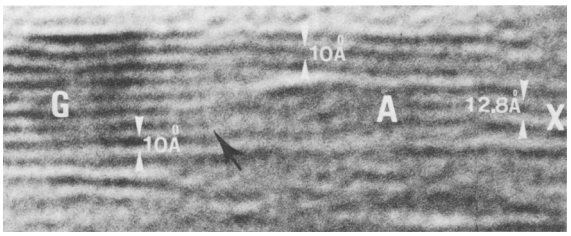

Figure 14. Lattice fringe image at the level of an elevated step (arrow) of a glauconite crystal (G). Note the transition of glauconite (d(001) ~ 10 Å) to noncrystalline material (A) to phase X (d(001) ~ 12.8 Å). Microtomed specimen.

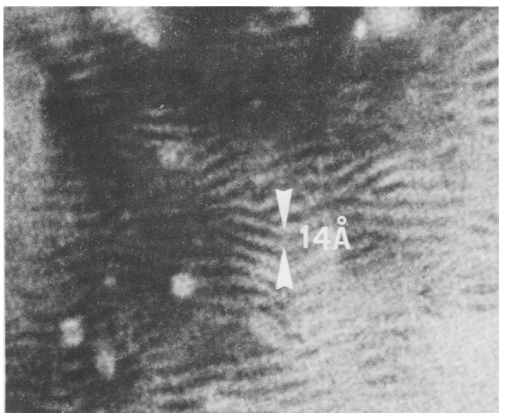

Figure 15. Lattice fringe image of smectite-like zone in a "glauconite" pellet showing many 00*l* lattice fringes (d(001) ~ 14 Å) altered by numerous edge dislocations. Ion-thinned specimen.

for glauconite explains the typical lamellar microstructure of the mineral as seen by SEM.

In addition, the gel-like material commonly surrounding the composite glauconite-X phase lamellae and the apparent transitional relationship between the gel and X, suggest that the X-phase may have formed from this gel.

CONCLUSIONS

In this work, new results about the structure and genesis of glauconite minerals have been obtained by high-resolution transmission electron microscopy.

1. Typical glauconite appears to have a characteristic mica structure (d(001) ~ 10 Å) and is never interstratified with other phases. The polytypic behavior (1*M*, 1*Md*) of this dioctahedral mica is similar to that of a trioctahedral mica. The $2M_1$ polytype, though rare, has been found for the first time. Its occurrence is possibly related to local chemical variations between one crystallite and another in the octahedral layer of the glauconite, making this stacking mode energetically possible.

2. The texture of the glauconite pellets, seen under normal (~100×) magnification, is characterized by a "spindle-arrangement" of the mica crystallites. These spindles form the automorphous lamellae of evolved glauconite grains. In the spindles, glauconite crystallites showing prominent growth features develop mainly along the long axis of the layers and parallel to each other by means of a layer-growth mechanism.

3. Inside the lamellae, an unidentified layered phase ("X" phase), with d(001) ~12.5 Å, genetically precedes the glauconite crystallites. The X phase is completely destabilized and transforms into a noncrystalline product, initially in the core of the lamellae where the mica grows preferentially.

4. Between the lamellae, extensive zones of noncrystalline material surround the X and mica phases. This material, comparable to a gel, is different from the noncrystalline decomposition product of the X phase.

5. Different stages of evolution towards the micaceous phase exist from one pellet to another, as well as from lamella to lamella in the same pellet. The evolution starts in the core and proceeds to the edge of the lamellae.

6. A smectite-like phase (d(001) ~ 14 Å), structurally different from the X phase, seems to be preferentially located in the outer part of the glauconite pellets. Its structural relations with the other phases could not be established.

In summary, the present study of glauconite pellets reveals that glauconitization constitutes an evolutionary process in which the earliest stage comprises the formation, probably from a gel, of a ~12.5-Å layered phase and its subsequent destabilization. Crystallization (neoformation) of a mica phase, i.e., glauconite *sensu stricto,* then occurs at the expense of the 12.5-Å phase. Whether the gel involved in these evolutive processes is a primary gel or whether it is a decomposition product of various starting minerals is presently unknown. From a structural point of view, the glauconitization process involves no mixed-layering phenomenon between the different crystallized phases. Furthermore, a continuous solid solution does not occur between these phases. Each glauconite pellet appears to be a mixture of authigenic layered minerals which, through decomposition and crystallization, evolve towards the same single mica lattice, i.e., glauconite *sensu stricto.*

ACKNOWLEDGMENTS

The authors are grateful to L. Aguirre, A. Baronnet, R. Boistelle, and B. Velde for their helpful discussion and critical comments on the manuscript.

REFERENCES

Amouric, M. and Baronnet, A. (1983) Effect of early nucleation conditions on synthetic muscovite polytypism as

seen by high resolution transmission electron microscopy: *Phys. Chem. Miner.* **9,** 146–159.

Amouric, M., Baronnet, A., and Finck, C. (1978) Polytypisme et désordre dans les micas dioctaédriques synthétiques. Etude par imagerie de réseau: *Mat. Res. Bull.* **13,** 627–634.

Amouric, M., Mercuriot, G., and Baronnet, A. (1981) On computed and observed HRTEM images of perfect mica polytypes: *Bull. Mineral.* **104,** 298–313.

Appelo, C. A. J. (1978) Aspects of mica-related clay minerals in hydrogeochemistry: Ph.D. thesis, Univ. Amsterdam, 75 pp.

Baronnet, A. (1974) Etude en microscopie électronique des premiers stades de croissance d'un mica synthétique, la phlogopite hydroxylée: *High Temp. High Press.* **6,** 193–198.

Baronnet, A., Amouric, M., and Chabot, B. (1976) Mécanismes de croissance, polytypisme et polymorphisme de la muscovite hydroxylée synthétique: *J. Cryst. Growth* **32,** 37–59.

Bentor, Y. K. and Kastner, M. (1965) Notes on the mineralogy and origin of glauconite: *J. Sed. Petrol.* **35,** 155–166.

Burst, J. F. (1958a) Mineralogical heterogeneity in "glauconite" pellets: *Amer. Mineral.* **43,** 481–497.

Burst, J. F. (1958b) "Glauconite" pellets: their mineral nature and applications to stratigraphic interpretations: *Bull. Amer. Assoc. Pet. Geol.* **42,** 310–327.

Charpy, N. and Nahon, D. (1978) Contribution à l'étude lithostratigraphique et chronostratigraphique du Tertiaire du Bassin de Côte d'Ivoire: *Rapp. Dép. Sc. Terre, Univ. Abidjian* **18,** 33 pp.

Cimbálniková, A. (1971a) Chemical variability and structural heterogeneity of glauconites: *Amer. Mineral.* **56,** 1385–1392.

Cimbálniková, A. (1971b) Influence of 10 Å–14 Å interlayering on the layer charge of glauconites: *Amer. Mineral.* **56,** 1393–1398.

De Gennes, P. G. (1974) *The Physics of Liquid Crystals:* Oxford Univ. Press, Oxford, 320 pp.

Eberhart, J. P. and Triki, R. (1972) Description d'une technique permettant d'obtenir des coupes minces de minéraux argileux par ultramicrotomie. Application à l'étude des minéraux argileux interstratifiés: *J. Microscop.* **15,** 111–120.

Ernst, W. G. (1963) Significance of phengitic micas from low-grade schists: *Amer. Mineral.* **48,** 1357–1373.

Giresse, P. and Odin, G. S. (1973) Nature minéralogique et origine des glauconies du plateau continental du Gabon et du Congo: *Sedimentology* **20,** 457–488.

Hower, J. (1961) Some factors concerning the nature and origin of glauconite: *Amer. Mineral.* **46,** 313–334.

Iijima, S. and Buseck, P. R. (1978) Experimental study of disordered mica structure by HREM: *Acta Crystallogr.* **A34,** 709–719.

Katsnel'son, Y. Y., Nyrkov, A. A., and Yakushev, V. V. (1978) Structural and chemical characteristics of glauconite as its qualitative indicators: *Lithol. Min. Res.* **13,** 324–335.

Kohler, E. E. (1980) The occurrence and properties of glauconites in Mesozoic and Cenozoic sediments in northwestern and southern Germany: *Geol. Jb.* **D39,** 115–136.

McRae, S. G. (1972) Glauconite: *Earth-Sci. Rev.* **8,** 397–440.

McRae, S. G. and Lambert, J. L. M. (1968) A study of some glauconites from Cretaceous and Tertiary formations in southeast England: *Clay Mineral.* **7,** 431–440.

Manghnani, M. H. and Hower, J. (1964) Glauconites: cation exchange capacities and infrared spectra: *Amer. Mineral.* **49,** 586–598.

Martin, L. (1972) Etude des "faecal-pellets" minéralisés des sédiments du plateau continental de Côte d'Ivoire: *Cah. ORSTOM, sér. Géol.* **4,** 105–120.

Nahon, D., Carozzi, A. V., and Parron, C. (1980) Lateritic weathering as a mechanism for the generation of ferruginous ooïds: *J. Sed. Petrol.* **50,** 1287–1298.

Odin, G. S. (1974) Application de la microscopie électronique par réflexion à l'étude des minéraux argileux: exemple des minéraux des glauconies: *Trav. Lab. Micropal., Univ. Paris* **3,** 297–313.

Odin, G. S. (1975) Les glauconies: constitution, formation, âge: Ph.D. thesis, Univ. Paris, 277 pp.

Odom, I. E. (1976) Microstructure, mineralogy and chemistry of Cambrian galuconite pellets and glauconite, central U.S.A.: *Clays & Clay Minerals* **24,** 232–238.

Oertel, G., Curtis, C. D., and Phakey, P. P. (1973) A transmission electron microscope and X-ray diffraction study in muscovite and chlorite: *Mineral. Mag.* **39,** 176–188.

Parron, C. and Nahon, D. (1980) Red bed genesis by lateritic weathering of glauconitic sediments: *J. Geol. Soc. London* **137,** 689–693.

Paulus, M., Dubon, A., and Etienne, J. (1975) Application of ion thinning to the study of the structure of argillaceous rocks by transmission electron microscopy: *Clays & Clay Minerals* **20,** 193–197.

Phakey, P. P., Curtis, C. D., and Oertel, G. (1972) Transmission electron microscopy of fine-grained phyllosilicates in ultra-thin rock sections: *Clays & Clay Minerals* **20,** 193–197.

Porrenga, D. H. (1967) Glauconite and chamosite as depth indicators in the marine environment: *Marine Geol.* **5,** 495–501.

Tchoubar, C., Rautureau, M., and Clinard, C. (1973) Technique d'inclusion appliquée à l'étude des silicates lamellaires et fibreaux: *J. Microsc.* **18,** 147–157.

Thompson, G. R. and Hower, J. (1975) The mineralogy of glauconite: *Clays & Clay Minerals* **23,** 289–300.

Velde, B. (1976) The chemical evolution of glauconite pellets as seen by microprobe determinations: *Mineral. Mag.* **40,** 753–760.

Velde, B. and Odin, G. S. (1975) Further information related to the origin of glauconite: *Clays & Clay Minerals* **23,** 376–381.

Warshaw, C. M. (1957) The mineralogy of glauconite: Ph.D. thesis, Pennsylvania State Univ., University Park, Pennsylvania, 155 pp.

Wermund, E. G. (1961) Glauconite in early Tertiary sediments of Gulf Coastal Province: *Bull. Amer. Assoc. Pet. Geol.* **45,** 1667–1696.

Wise, W. S. and Eugster, H. P. (1964) Celadonite: synthesis, thermal stability and occurrence: *Amer. Mineral.* **49,** 1031–1083.

Yoder, H. S. and Eugster, H. P. (1955) Synthetic and natural muscovites: *Geochim. Cosmochim. Acta* **8,** 225–280.

(Received 24 April 1984; accepted 10 March 1985; Ms. 1357)